Conf-811145--13

CONF-811145--13

DE83 003503

A TEM STUDY OF NEUTRON-IRRADIATED IRON*

L. L. Horton, J. Bentley, and K. Farrell

Metals and Ceramics Division, Oak Ridge National Laboratory
Oak Ridge, TN 37830

ABSTRACT

The results of a transmission electron microscopy study of the defect structure in iron neutron-irradiated to low fluences (< 1 dpa) at temperatures of 455 to 1013 K are presented. The dislocation microstructures coarsen with increasing irradiation temperature from decorated dislocations, through clusters of dislocation loops, to near-edge, interstitial dislocation loops with $\underline{b} = a\langle 100\rangle$, and network segments. Significant cavity formation occurred only at 548 to 723 K, with homogeneous distributions found only at 623 and 673 K. The maximum swelling of 0.07% occurred at 673 K. Large cavities had a truncated octahedral shape with {111} facets and {100} truncations. Damage halos were observed around boron-containing precipitates. The effects of interstitial impurities on microstructural development and the differences in the observed microstructures compared to those in refractory bcc metals are discussed.

*Research sponsored by the Division of Materials Sciences, U.S. Department of Energy, under contract No. W-7405-eng-26 with Union Carbide Corporation.

1. INTRODUCTION

Ferritic steels are currently being considered as candidate structural materials for cladding and duct applications in fast breeder reactors and for first wall and blanket applications in proposed fusion reactors. One reason for this interest is the low swelling observed in neutron-irradiated ferritic steels [1–11]. The reason for the swelling resistance of these steels is not completely understood. Characterization of the radiation-induced secondary defect structures, essential to understanding the mechanisms of radiation damage, is incomplete. The lack of microstructural data is partially due to the difficulties associated with transmission electron microscopy (TEM) examinations of ferromagnetic materials. These difficulties are enhanced by the usually complex preirradiation microstructures of many of the steels of interest. Analyses of the dislocation microstructures, for example, have been reported for only one study of neutron-irradiated ferritic steel [10,11].

However, iron and many of the simple bcc iron alloys which form the basis of the more complex steels possess swelling characteristics similar to those observed in ferritic steels. Detailed analyses of the defect structures have been reported for various irradiation temperatures and fluences for neutron [9–15], heavy ion [15–20], and electron [21–23] irradiated iron, as well as for neutron [9–12] and heavy ion [18] irradiated iron-chromium alloys. These studies have provided valuable information relevant to the mechanisms of radiation damage for ferritic steels. In addition, results from these investigations have established a partial foundation for the more complex analyses required for the steels.

The purpose of the current investigation is to study the secondary defect structures which form at temperatures of 455 to 1013 K in iron neutron-irradiated to 0.5 to 1 dpa (displacements per atom). In addition to characterization of the dislocation and cavity microstructures, damage halos found around boron-containing precipitates were also examined.

2. EXPERIMENTAL PROCEDURE

2.1 Specimen Material

The specimens used for this investigation were fabricated from two-pass zone-refined FerroVac-E iron. The chemical analysis for the iron is presented in Table I. Disk specimens (3-mm diameter) were mechanically punched from a rolled, 0.5-mm-thick sheet of this material, and were then annealed at 1025 K (750°C) for 1 hour at a pressure <1 mPa (10^{-5} torr).

TEM examinations of the unirradiated specimens revealed a low dislocation density of $<10^{11}$ m^{-2}. Texture was apparent in the specimens with many grains having a foil normal near <111>. A low concentration of precipitates, believed to be B_4C, was observed in the specimens.

2.2 Irradiation

The iron disks were irradiated in helium-filled, stainless steel capsules in the Oak Ridge Research Reactor (ORR) during Run 228. The temperature of each capsule was monitored by thermocouples. Flux monitors were used to measure the neutron fluence during the experiment. Details of the experiment assembly for ORR-228 can be found elsewhere [24]. The irradiation parameters for the iron specimens are listed in Table II. The damage levels (dpa) were calculated from the fast fluence ($E > 0.1$ MeV), assuming a threshold displacement energy of 40 eV, and using the ORR spectral information provided by Gabriel et al.[25].

2.3 TEM Specimen Preparation and Examination

The neutron-irradiated specimens were electropolished using the two-step semiautomatic method developed by DuBose and Stiegler [26]. A standard A-2 electrolyte (700 ml ethyl alcohol, 100 ml butylcellusolve, 125 ml distilled water, and 78 ml perchloric acid) was used.

The specimens were examined in a JEM 120C TEM equipped with a special objective lens pole-piece (AMG) for the observation of magnetic materials [27]. This pole-piece allows high-angle tilting experiments, such as those required for dislocation loop analyses, to be performed. When required by the coarseness of the defect distribution the specimens were also examined in a Hitachi 1 MV high voltage electron microscope (HVEM).

3. RESULTS

3.1 Dislocation Microstructures

The dislocation microstructures can be classified as belonging to one of four groups corresponding to four irradiation-temperature ranges. Within any one group the structures were qualitatively similar. Each temperature range and its corresponding microstructures are presented separately.

For the lowest temperature range, 455 to 523 K, the dislocation component of the microstructure was primarily limited to small defect clusters formed near preirradiation dislocation segments. Representative micrographs of the structure in this group are shown in Fig. 1. At 455 K, a fairly homogeneous background of "blackspot" defects less than 6 nm diameter was also observed. The concentration of these defects was $\sim 10^{22}$ m^{-3}.

Based on the assumption that the small defects were small dislocation loops, a Burgers vector, $\underline{b}$, determination was attempted using the black-white image contrast of the defect. However, due to the presence of an unavoidable surface oxide and the usual problems associated with microscopy of magnetic specimens, the results were inconclusive.

In the second temperature group, 548 and 573 K, clusters of small loops were observed. Microstructures typical of those observed at these temperatures are shown in Fig. 2. The individual loops making up each cluster can be seen clearly in the enlarged inset of Fig. 2(b). Individual clusters were not associated with either precipitates or dislocation segments. However, a higher density of clusters and individual dislocation loops were observed at low-angle grain boundaries and at preirradiation dislocation segments.

The quantitative data (average loop diameter, d_L; average number of loops per cluster, N_L/cluster; average cluster diameter, $d_{cluster}$; cluster concentration, $C_{cluster}$; and dislocation density, ρ) for these structures, at each irradiation temperature, T_I, are shown in Table III. Some of these parameters were difficult to measure and the approximate values are presented only as a guide.

Due mainly to the high loop density, only a partial analysis of the loops in the clusters was possible. This analysis showed that the individual clusters were made up of loops with different Burgers vectors. Not all loops within a cluster showed the same residual contrast behavior. For diffracting vectors, $\underline{g}$ = <110> at beam directions, $\underline{z}$ near <001>, many of the individual loops appeared to be in a near edge-on orientation on {100}. Based on this observation, it was assumed that many of the loops were near-edge with $\underline{b}$ = a<100>. "Inside-outside"

contrast analysis with $\underline{g} \cdot \underline{b} = \pm 2$ indicated that the analyzable loops were interstitial in nature. Another conclusion, based on the observed variation in cluster shape during high-angle tilting experiments, was that the clusters of loops are approximately equiaxed and certainly not planar arrays.

The third temperature range was 623 to 773 K, for which a fairly homogeneous distribution of loops and network segments was present. Representative areas from specimens irradiated at 623, 673, 723, and 773 K are shown in Fig. 3. The extremely coarse distribution at 773 K required examination in an HVEM to obtain a true impression of the microstructure. As shown in Fig. 3, many loops intersect the specimen surfaces. At 723 and 773 K, unidentified precipitates were present near the center of most loops. This can be seen clearly in Fig. 3(d), an HVEM micrograph.

The measured quantitative data for the loop structures are presented in Table IV and Fig. 4. The average loop diameter, d_L, increases and the loop concentration, C_L, decreases with increasing temperature. Also, the total dislocation density (including loops) decreases by about an order of magnitude for each 50° temperature increase.

Analyses of the geometry and nature of the dislocation loops were performed following the techniques of Maher and Eyre [28]. An example of an analysis for a specimen irradiated at 623 K is illustrated in Fig. 5. In this figure, the loops that were analyzed are labeled alphabetically. In Fig. 5(a) ($\underline{g} = [1\bar{1}0]$, $\underline{z}$ near [001]) the majority of the loops are in a near edge-on orientation with the loop images aligned perpendicular to the [100] and [010] directions. A similar observation

was made for $\underline{g} = [\bar{1}01]$ with $\underline{z}$ near [010]. These observations indicate that the loops are near-edge, on {100} planes and with $\underline{b} = a\langle 100\rangle$. This conclusion was substantiated by micrographs taken with $\underline{g} = \langle 110\rangle$ for $\underline{z}$ near [111], as shown in Fig. 5(b,c and d), and $\underline{g} = \langle 200\rangle$ for $\underline{z}$ near [001] and [010]. In these micrographs, the majority of the dislocation loop images showed residual contrast for diffracting conditions appropriate for $\underline{b} = a\langle 100\rangle$. The nature of the loops was then determined by the "inside-outside" contrast criterion using $\underline{g}\cdot\underline{b} = \pm 2$ diffraction conditions and working in "safe orientations" [28]. An example is shown in Fig. 5(e and f). For loops with $\underline{b} = a[010]$ (loops B - H), "outside" contrast is observed in Fig. 5(e), ($\underline{g} = [\bar{1}2\bar{1}]$, $\underline{g}\cdot\underline{b} = +2$), and "inside" contrast is observed in Fig. 5(f) ($\underline{g} = [1\bar{2}1]$, $\underline{g}\cdot\underline{b} = -2$),indicating that these are interstitial loops. In these same micrographs, loops with $\underline{b} = a[100]$ (loops labeled I - K) and $\underline{b} = a[001]$ (loops L - O) have "inside" contrast in Fig. 5(e) and "outside" contrast in Fig. 5(f), showing that these are interstitial loops as well. This conclusion was confirmed by micrographs taken with the appropriate $\underline{g}\cdot\underline{b} = \pm 2$ diffracting conditions.

Only one loop, labeled A in Fig. 5, was determined not to have $\underline{b} = a\langle 100\rangle$; it had $\underline{b} = a/2[\bar{1}11]$ and was interstitial in nature. Similar loop analyses were performed for loops formed at irradiation temperatures of 673 and 723 K. At these temperatures all loops analyzed were of near-edge character with $\underline{b} = a\langle 100\rangle$ and were interstitial in nature.

In the fourth temperature range, 923 and 1013 K, there was no observable difference in the dislocation microstructure as compared to that found in unirradiated specimens.

3.2 Cavity Microstructures

Significant cavity formation occurred over a limited irradiation temperature range of 548 to 723 K. The cavity microstructures present at these irradiation temperatures are shown in Fig. 6. The cavity distribution is homogeneous only at 623 and 673 K. At 548 and 573 K, the cavities are found in association with the clusters of dislocation loops. This observation is a clear example of the cooperative growth of cavities and interstitial dislocation loops. The association can be clearly seen in the enlarged inset of Fig. 6(a). No grain boundaries were observed in the thin regions of these specimens, so no relationship between grain boundaries and cavities could be determined.

At 773 K, cavities were very sparse and were observed only in association with unidentified precipitates (probably carbides), as shown in Fig. 7. Similar cavity-precipitate association was sometimes observed in the specimen irradiated at 723 K. At 923 K, excluding the damage halos, only a few cavities, located on grain boundaries, were observed.

Facets on the larger cavities were clearly visible, but for the small cavities no conclusions in regard to their shape could be reached. Suprisingly, detailed tilting experiments showed that the faceted cavities were {111} octahedra with {100} truncations. The cavity diameters were measured assuming a circular projection with the same area as the observed crystallographic shape.

The quantitative cavity data are summarized in Table V and Fig. 8. The volume-averaged cavity diameter, d_c, reaches a maximum of ~12 nm at 673 K. The cavity concentration, C_c, is a maximum of $\sim 10^{21}$ m^{-3} at irradiation temperatures of 573 to 673 K. The calculated maximum swelling or cavity volume fraction (CVF) of ~0.07% occurs at 623 and 673 K.

3.3 Halo Microstructures

Damage halos centered on B_4C precipitates were observed in specimens irradiated at 493, 523, 723, and 923 K. The low concentration of halos ($<10^{11}$ m^{-3}) allowed them to be considered as a separate feature of the microstructure. Damage halos are formed by energetic recoil products from the (n,α) transmutation reaction of ^{10}B:

$$^{10}B + {}^{1}n_{th} \rightarrow {}^{4}\alpha\ (1.47\ MeV) + {}^{7}Li\ (0.84\ MeV).$$

More detailed discussions of halo formation have been presented elsewhere [29-31]. The range of 0.84 MeV Li in Fe is 1.3 μm [32]. The range of 1.47 MeV α-particles in Fe is 2.4 μm [33]. Halos are believed to result largely from the impurity effect on the bulk neutron displacement damage. The type of damage-clusters in the halos depends on the irradiation temperature. The appearance of a halo in a thinned section further depends on where the foil intersects the spheres of damage surrounding the precipitate, and the size and boron content of the precipitate. For example, the larger the precipitate the larger the outside diameter and width of the individual halos.

At 493 and 523 K, double halos of small dislocation loops were observed. At 723 K, the two halos were not distinct in any of the observed halos and the microstructure consisted of larger dislocation loops. At 923 K, the halo microstructure consists of a high concentration of small cavities with no associated dislocation structure. For comparison, each of these types of halo structure is presented in Fig. 9.

The diameters of the lithium and helium halos were measured on micrographs of foils irradiated at 493 and 523 K in which both the halos and the precipitate that formed the halos were observed. The diameters

measured were those defined by the center of the halo damage region. The average diameter of the Li halo was ~2.5 μm and the diameter of the He halo was ~5.2 μm. These average measurements correlate well with the calculated values.

A partial analysis of the dislocation loops within a He halo formed at 523 K indicated that loops with both $\underline{b}$ = a<100> and $\underline{b}$ = a/2<111> were present. Analysis of the loops in the halos found in the foil irradiated at 723 K demonstrated that all of the loops were near edge with $\underline{b}$ = a<100> and were interstitial in nature. Part of this analysis is shown in Fig. 10.

A comparison of the quantitative dislocation parameters for halo and non-halo regions for the specimen irradiated at 723 K is presented in Table VI. While the loops in both regions are interstitial with $\underline{b}$ = a<100>, the loops in the halos are smaller and have a factor of 30 higher concentration than the loops not found in halos. The total dislocation density was an order of magnitude higher in the halos.

At 923 K, two concentric diffuse cavity halos were observed. The halos are shown in Fig. 11 which is an enlargement of an area across the two halos shown in Fig. 9. The cavities in the inner (lithium) halo are larger and have a lower concentration than those in the outer (helium) halo. A few cavities were observed in the regions surrounding the halo. Near the halos, cavities form on and near grain boundaries. The cavities on the boundary are about a factor of 2 larger than those within the halo.

4. DISCUSSION

The observations of the damage microstructures for low-dose, neutron-irradiated iron differ significantly from the structures observed in other bcc materials. In particular, the observations of decorated dislocations, clustered dislocation loops, a<100> interstitial loops, cavity shape and low swelling merit further discussion.

While the observation of decorated dislocations is not unique, this feature has not been reported previously for irradiated bcc materials. Preferential clustering of defects at dislocation lines has been observed in low-fluence, neutron-irradiated copper for irradiation temperatures of 0.21 T_m to 0.5 T_m, where T_m is the absolute melting temperature [34,35]. In the present work, decorated dislocations were observed for irradiation temperatures from 0.25 to 0.29 T_m. The nucleation of defect clusters at dislocations is believed to be promoted by the strain field of the dislocation [35]. The presence of a Cottrell atmosphere at the dislocations, a well-known phenomenon in iron, could further enhance cluster formation by trapping interstitials and preventing their absorption by the dislocations. Once a cluster is formed, its strain field could promote further cluster formation nearby [35].

The general appearance of the clusters of dislocation loops in iron is similar to the "rafts" of small dislocation loops and "black-spot" clusters observed in other neutron-irradiated bcc materials such as molybdenum [36–38], TZM [37–40], and tungsten [41]. For the studies of molybdenum, TZM, and tungsten, detailed analyses of raft geometry and loop characteristics have been reported. In these materials, rafts form on {111} planes. The thickness of the rafts is 10-20 nm (a few loop

diameters). All of the loops within a raft have the same a/2<111> Burgers vector [37]. The loops are assumed to be interstitial in nature. The clusters of loops in iron differ from these rafts in several aspects. In iron, the clusters are not planar features. Also, many of the loops within the clusters were near-edge interstitial dislocation loops with $\underline{b}$ = a<100>. Unlike rafts, all of the loops within an individual cluster did not have the same Burgers vector.

Rafts in refractory bcc metals are believed to form by dislocation loops with the same Burgers vectors gliding together as a result of the elastic interactions between the loops [36,38,42]. A similar interaction which is not limited to loops of the same Burgers vector could be responsible for the formation of clusters of loops in iron. However, loops with $\underline{b}$ = a<100> are believed to have a higher glide stress than loops with $\underline{b}$ = a/2<111>. Therefore, a more complex mechanism may be responsible for the cluster formation in iron. Further work is clearly needed to understand the reasons for and the mechanisms of the formation of these clusters.

One of the surprising features of the radiation-induced microstructures in iron [9–12,17,19,21] and ferritic steels [9–11,43] is the common observation that virtually all of the dislocation loops formed during irradiation at elevated temperatures are near-edge, interstitial loops with $\underline{b}$ = a<100>. The results of the current investigation are in agreement with these observations. Only in the halos formed at the lower irradiation temperature of 523 K did the loops have both $\underline{b}$ = a<100> and $\underline{b}$ = a/2<111>. The interstitial loops observed in other irradiated bcc materials commonly are oriented near-edge with $\underline{b}$ = a/2<111>. The formation in bcc metals of loops with either $\underline{b}$ = a<100> (at elevated temperatures) or the more energetically favored

$\underline{b}$ = a/2<111> is accounted for in the model of Eyre and Bullough [44]. However, the model does not account for the presence of solely $\underline{b}$ = a<100> loops. Since the formation of a/2<111> loops is energetically favored, the majority of the loops should have $\underline{b}$ = a/2<111>. Recently, the relative probability of the formation of loops with $\underline{b}$ = a<100> and $\underline{b}$ = a/2<111> in bcc materials has been further examined [10,11]. These calculations have shown that for iron the relative probability of forming loops with $\underline{b}$ = a<100> as compared to $\underline{b}$ = a/2<111>, while higher than for many other bcc materials, is still quite low ($\sim 5.7 \times 10^{-9}$). A satisfactory explanation for the occurrence of dislocation loops with solely $\underline{b}$ = a<100> in irradiated iron is not currently available. Understanding this aspect of the radiation-induced microstructure is important, especially since the formation of loops with $\underline{b}$ = <100> is claimed to be related to the low-swelling characteristics of iron and ferritic steels [10,11].

The observed cavity shape, a truncated octahedron with {111} facets and {100} truncations, is the shape usually found in fcc materials. The expected and commonly observed shape in bcc materials is a truncated 12-faced polyhedron with {110} facets and {100} truncations. This latter shape has been observed previously in neutron-irradiated iron [14]. Truncated octahedral cavities have also been observed in ion-irradiated iron and iron-chromium alloys [19]. The reason for this unexpected cavity shape is under further study, but is possibly related to surface energy variations caused by impurities preferentially segregating to a specific set of planes, or is a result of non-equilibrium conditions during cavity growth.

The low swelling observed in this study is consistent with previously reported results for ferritic materials mentioned in the

introduction. Generally, little data exist on the swelling of neutron irradiated iron, but for irradiations to 30 and 23 dpa swelling maxima were observed at ~700 K (~420°C) and ~780 K (~510°C), respectively [9,12]. However, it should be noted that the 30 dpa irradiation was not performed for irradiation temperatures above ~730 K, and the 23 dpa irradiation was not performed for irradiation temperatures below ~710 K. In the current investigation the peak swelling was observed at 673 K, in approximate agreement with the results for the 30 dpa irradiation. However, at 773 K, the approximate location of the 23 dpa swelling maximum, the swelling in the present work was too small for accurate measurement. While these comparisons may indicate a shift in the peak swelling to higher irradiation temperatures with increased fluence, further work is again clearly required.

The few cavities found on the grain boundaries in the non-halo regions of the specimen irradiated at 923 K are probably helium bubbles. A small concentration of helium is formed in iron from the transmutation reaction: $^{56}Fe(n,\alpha)^{53}Cr$. For the current irradiation, the concentration of helium from this reaction is only ~0.22 at. ppm [29].

The observation of damage halos in iron presents another interesting aspect of the radiation-induced microstructures. At all of the irradiation temperatures, the defect clusters in the halos varied significantly from those in non-halo regions. These differences may be caused by the higher displacement damage, damage rates or helium and lithium concentrations in the halo regions. While it is impossible to assign a single cause to the microstructural features observed in the halos it is believed that the higher He and Li concentrations have the strongest effect. Ion-irradiation studies of austenitic materials have

shown that preimplanted and coimplanted helium can enhance cavity and interstitial dislocation loop formation [45]. The characteristics of the high-temperature halos are probably influenced by the presence of helium. At these temperatures, except for a few cavities at grain boundaries, cavities were observed only within or near the halos. While the higher displacement damage in the halos is undoubtedly a contributing factor, the helium is probably more important in aiding cavity formation. Cavity formation in regions outside the main halo regions is probably due to the diffusion of helium away from the halo. This "spread" of cavities away from the main damage regions is responsible for the rather diffuse appearance of the halos.

A similar temperature dependence of the halo microstructures has been observed in neutron-irradiated iron specimens that were doped with B_4C precipitates [46]. These specimens were also irradiated in ORR-228 in the same capsules as the iron used for this study. In the Fe-B_4C specimens, due to the higher precipitate concentration, halos were found at all irradiation temperatures. Presumably halos were present in all of the presently-investigated iron specimens as well, but, due to the low precipitate concentration, the halos were not found in the electron-transparent regions of all of the specimens.

The present observations have revealed a low point defect retention in clusters compared to other bcc and fcc metals of similar purity and suggest a strong effect of impurities on the microstructural development by the trapping of point defects and segregation to defect clusters. Since the concentration of metallic impurities is low, the observed effects are considered most likely to be due to carbon. As discussed earlier, the clustering of defects at preirradiation dislocation

segments for irradiation temperatures of 455–523 K is probably related to Cottrell atmospheres at the dislocations. At 548 and 573 K, the higher concentration of loop clusters found at dislocations is probably also related to these impurity clouds. For irradiation temperatures of 623 to 773 K, many of the dislocation loops intersect the foil surfaces without gliding out. The majority of the loops observed at these temperatures had $\underline{b} = a\langle 100\rangle$. Since loops with $\underline{b} = a\langle 100\rangle$ are less glissile than loops with $\underline{b} = a/2\langle 111\rangle$, the image forces may not be sufficient to cause the loops to glide from the foil. However, the presence of Cottrell atmospheres could also cause the loops to be pinned and thus prevent them from gliding out of the foil. Finally, for irradiation temperatures of 723 K or higher, small precipitates, presumed to be carbides, are found in the center of the dislocation loops.

5. SUMMARY

This study of neutron damage in iron irradiated to low dose at controlled temperatures has revealed:

(1) The dislocation microstructures coarsen with increasing irradiation temperature, developing from decorated dislocations (T_I = 455 to 523 K), through clusters of loops (T_I = 548 and 573 K), to loops and network segments (T_I = 623 to 773 K). At higher temperatures no change in the dislocation structures were evident.

(2) Significant cavity formation occurs for T_I = 548 to 723 K. Cavity volume fractions are <0.1%.

(3) Large cavities are faceted {111} octahedra with {100} truncations.

(4) Near-edge, interstitial dislocation loops with $\underline{b} = a\langle 100\rangle$ are

the predominant feature of the dislocation loop microstructures.

(5) Damage halos result from $^{10}B(n,\alpha)^{7}Li$ reactions.

(6) The damage microstructures in iron and refractory bcc metals are qualitatively different.

(7) The observations indicate a low point defect retention in clusters and suggest a strong effect of impurities upon microstructural development due to trapping and segregation.

(8) These results are expected to be useful in the study of the more complex ferritic steels.

Acknowledgments

The authors would like to thank J. T. Houston for preparation of the specimens, J. W. Woods and W. W. Davis for assistance in the planning and assembly of ORR-228, Drs. E. A. Kenik and N. H. Packan for technical comments, and Frances Scarboro for manuscript preparation.

References

[1] D. S. Gelles, Proc. of Second Topical Meeting on Fusion Reactor Materials (Seattle, WA, Aug. 9–12, 1981); to be published in Journal of Nuclear Materials.

[2] R. W. Powell, D. T. Peterson, M. K. Zimmerschied, and J. F. Bates, ibid.

[3] E. A. Little, D. R. Arkell, D. R. Harries, B. R. Lewthwaite, and T. M. Williams, pp. 31–37 in Proc. of Inter. Conf. on Irradiation Behavior of Metallic Materials for Fast Reactor Core Components, ed. by J. Poirier and J. M. DuPouy (held at Ajaccio, Corsica, France, 1979).

[4] J. Erler, A. Maillard, G. Brun, J. Lehmann, and J. M. DuPouy, ibid., pp. 11–16.

[5] J. J. Huet, A. DeBremaecker, M. Snykers, Ph. Van Asbroeck, and W. Vandermeulen, ibid., pp. 5–9.

[6] K. R. Garr, C. G. Rhodes, and D. Kramer, ASTM-STP-529 (ASTM, Baltimore, MD, 1973), pp. 109–118.

[7] J. J. Huet, A. Delbrassine, Ph. Van Asbroeck, and J. Vandermeulen, pp. 357–365 in Radiation Effects in Breeder Reactor Structural Materials, ed. by M. L. Bleiberg and J. W. Bennett (TMS-AIME, 1977).

[8] V. I. Sherbak, V. N. Bykow, A. N. Vorobiew, and V. D. Dmitriew, ibid., pp. 773–779.

[9] E. A. Little and D. A. Stow, J. Nucl. Mater. 87 (1979) 25–39.

[10] E. A. Little, R. Bullough, and M. H. Wood, Proc. Roy. Soc. London, A372 (1980) 565–579.

[11] R. Bullough, M. H. Wood, and E. A. Little, ASTM-STP-725 (ASTM, Baltimore, MD, 1981), pp. 593–609.

[12] E. A. Little and D. A. Stow, op. cit. [3], pp. 17–24.

[13] K. Farrell and J. T. Houston, J. Nucl. Mater. 35 (1970) 352–355.

[14] G. L. Kulcinski, B. Mastel, and J. L. Brimhall, Rad. Effects 2 (1969) 57–59.

[15] E. A. Smidt, Jr., J. A. Sprague, J. E. Westmoreland, and P. R. Malmberg, pp. 341–362 in Defect and Defect Clusters in BCC Metals and Their Alloys, ed. by R. J. Arsenault (National Bureau of Standards, Maryland, 1973).

[16] M. L. Jenkins, C. A. English, and B. L. Eyre, Phil. Mag. 38 (1978) 97–114.

[17] B. C. Masters, Phil. Mag. 11 (1965) 881–893.

[18] L. L. Horton, J. Bentley, and W. A. Jesser, Proc. of Second Topical Meeting on Fusion Reactor Materials (Seattle, WA, Aug. 9–11, 1981); to be published in Journal of Nuclear Materials.

[19] L. L. Horton, J. Bentley, and W. A. Jesser, ibid.

[20] E. Kuramoto, N. Yoshida, N. Tsukuda, K. Kitajima, N. H. Packan, M. B. Lewis, and L. K. Mansur, ibid.

[21] E. A. Little and B. L. Eyre, AERE-R7095, Harwell, England, 1972.

[22] K. Kitajima, K. Futagami, and E. Kuramoto, J. Nucl. Mater. 85&86 (1979) 725–729.

[23] E. Kuramoto, K. Futagami, and K. Kitajima, pp. 589–592 in Proc. of Fifth Inter. Conf. on HVEM (held in Kyoto, Japan, 1977).
[24] L. L. Horton, Ph.D. dissertation, University of Virginia (January 1982).
[25] T. A. Gabriel, B. L. Bishop, and F. W. Wiffen, Calculated Irradiation Response of Materials Using Fission Reactor (HFIR, ORR and EBR-II) Neutron Spectra, ORNL/TM-6361 (August 1979).
[26] C.K.H. DuBose and J. O. Stiegler, Rev. Sci. Instr. 38(5) (May 1967) 694–695.
[27] K. Shirota, A. Yonezawa, K. Shibatomi, and T. Yanaka, Proc. of 34th Annual EMSA Meeting (1976), pp. 540–541.
[28] D. M. Maher and B. L. Eyre, Phil. Mag. 23 (1971) 409–438.
[29] D. A. Woodford, J. P. Smith, and J. Moteff, J. Nucl. Mater. 24 (1967) 118–120.
[30] D. S. Gelles and F. A. Garner, J. Nucl. Mater. 85&86 (1979) 689–693.
[31] R. C. Rau and R. L. Ladd, J. Nucl. Mater. 30 (1969) 297–302.
[32] U. Littmark and J. F. Ziegler, p. 211 in Handbook of Range Distributions for Energetic Ions in All Elements, ed. by J. F. Ziegler (Pergamon Press, Elmsford, NY, 1980).
[33] J. F. Ziegler, Helium Stopping Powers and Ranges in All Elemental Matter (Pergamon Press, Elmsford, NY, 1977).
[34] G. P. Scheidler, M. J. Makin, F. J. Minter, and W. F. Schilling, pp. 405–418 in The Nature of Small Defect Clusters, ed. by M. J. Makin (Her Majesty's Stationery Office, England, 1966).
[35] L. D. Hulett, Jr., T. O. Baldwin, J. C. Crump III, and F. W. Young, Jr., J. Appl. Phys. 39 (July 1968) 3945–3954.
[36] J. L. Brimhall and B. Mastel, Rad. Eff. 3 (1970) 203–215.
[37] J. Bentley, Ph.D. dissertation, University of Birmingham, England, 1974.
[38] J. Bentley, B. L. Eyre, and M. H. Loretto, pp. 925–931 in Fundamental Aspects of Rad. Damage in Metals, CONF-751006-P2, ed. by M. T. Robinson and F. W. Young, Jr. (NTIS, Springfield, VA, 1972).
[39] J. Bentley, B. L. Eyre, and M. H. Loretto, pp. 297–311 in Rad. Effects and Tritium Technology for Fusion Reactors, Vol. I, CONF-750989, ed. by F. W. Wiffen and J. S. Watson (NTIS, Springfield, VA, 1976).
[40] A. G. Pard and K. R. Garr, ibid., pp. 312–322.
[41] V. K. Sikka and J. Moteff, J. Nucl. Mater. 46 (1973) 217–219.
[42] B. L. Eyre, op. cit. [38], pp. 729–763.
[43] E. A. Little, Rad. Effects 16 (1972) 135–137.
[44] B. L. Eyre and R. Bullough, Phil. Mag. 12 (1965) 31–39.
[45] K. Farrell, Rad. Effects 53 (1980) 175–194.
[46] K. Farrell, unpublished results.

Table I. Chemical Analysis for the Iron Specimens Irradiated in ORR-228

Element	(wt ppm)	Element	(wt ppm)	Element	(wt ppm)	Element	(wt ppm)
C	30	Bi	1	Mg	<5	Si	90
H	7	Br	1	Mn	3	Ta	1
N	4	Ca	20	Na	10	Ti	0.3
O	8	Cl	60	Nb	<1	V	1
Al	75	Cr	3	Ni	180	W	3
As	0.4	Cu	5	P	5	Zn	<1
B	2	K	<1	S	15	Fe	Major

Table II. Irradiation Parameters for the Iron Specimens Irradiated in ORR-228

Temperature		Fluence, 10^{25} neutrons-m^{-2}			Damage Level
(K)	(°C)	Total	Fast (> 0.1 MeV)	Thermal (2200 m/s)	(dpa)
455	(182)	3.65	1.13	1.16	0.84
493	(220)	3.65	1.13	1.16	0.84
523	(250)	4.26	1.17	1.21	0.87
548	(275)	4.00	1.29	1.19	0.96
573	(300)	3.65	1.05	1.14	0.78
623	(350)	3.70	1.18	1.17	0.88
673	(400)	3.70	1.32	1.20	0.98
723	(450)	3.50	1.26	1.15	0.94
773	(500)	3.27	1.02	1.03	0.74
923	(650)	2.25	0.69	0.75	0.51
1013	(740)	3.35	0.87	0.95	0.64

Table III. Quantitative Data for Dislocation Microstructures Observed at 548 and 573 K

T_I (K)	d_L (nm)	N_L/cluster	$d_{cluster}$ (nm)	$C_{cluster}$ (10^{19} m^{-3})	ρ (10^{13} m^{-2})
548	~10	~20	150	9	9
573	~10	~15	100	15	13

Table IV. Dislocation Density and Loop Parameters for Intermediate Irradiation Temperatures

T_I (K)	C_L (10^{18} m^{-3})	d_L (nm)	ρ (m^{-2})
623	540	43	1×10^{14}
673	3.2	160	1.8×10^{13}
723	1.7	200	2.2×10^{12}
773	0.14	600	3.0×10^{11}

Table V. Quantitative Cavity Data for Neutron-Irradiated Iron

T_I (K)	d_c (nm)	C_C (10^{20} m^{-3})	CVF (%)
548	5.7	6.4	0.006
573	8.5	9.8	0.032
623	10.5	11	0.067
673	12.0	8.2	0.073
723	10.2	0.77	0.004

Table VI. Dislocation Density and Loop Parameters for Halo and Non-Halo Areas of a Specimen Irradiated at 723 K

	C_L (10^{18} m^{-3})	d_L (nm)	ρ (m^{-2})
Non-halo	1.7	200	2.2×10^{12}
He-halo	58	140	2×10^{13}

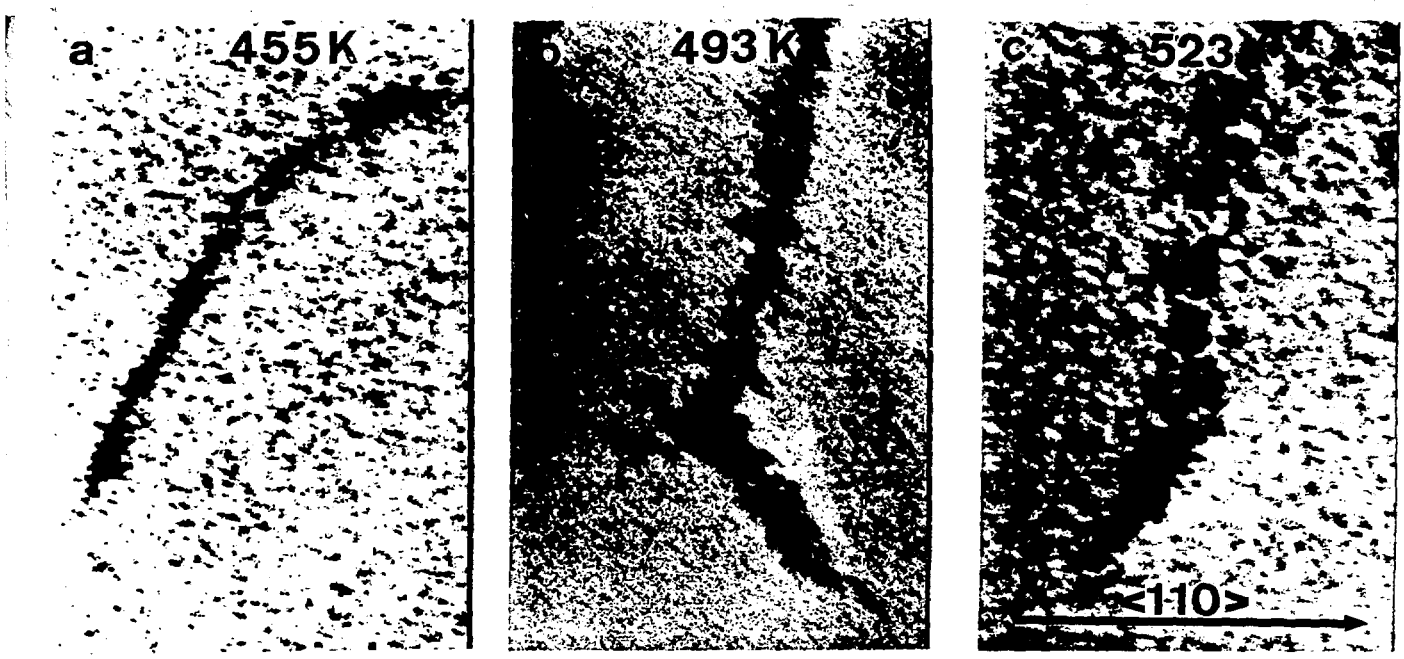

Fig. 1. Decorated dislocations observed for irradiation temperatures of 455 to 523 K. $\underline{g}$ is indicated by the arrow; the length of the arrow equals 500 nm. $\underline{z} \sim \langle 111 \rangle$.

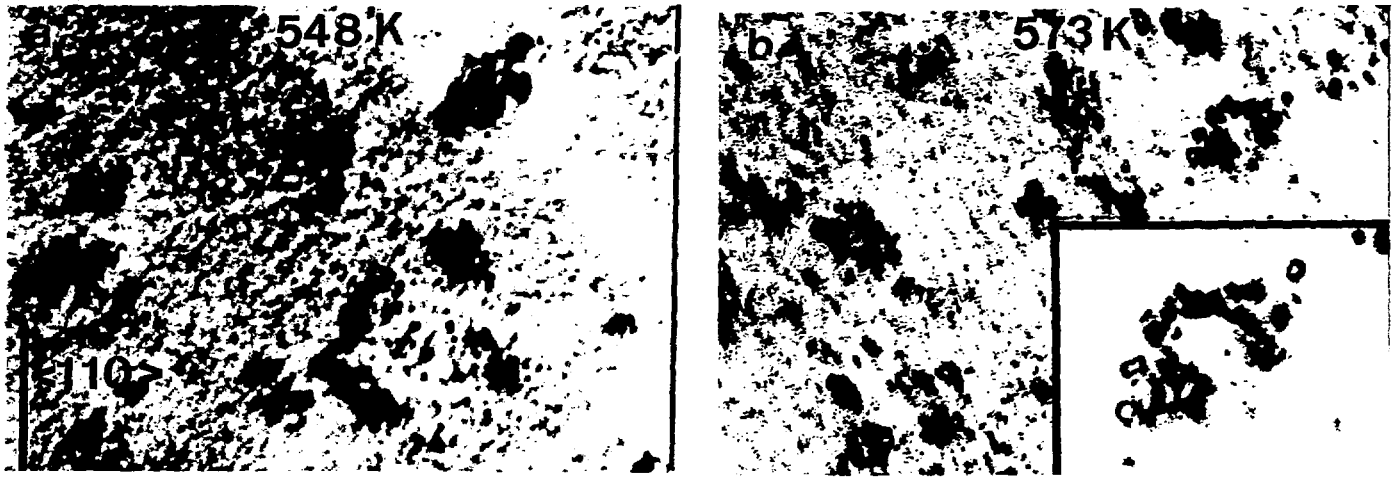

Fig. 2. Clusters of small loops observed for irradiation temperatures of 548 and 573 K. Inset is a 2× enlargement. $\underline{g}$ is indicated by the arrow; the length of the arrow equals 200 nm. $\underline{z} \sim \langle 111 \rangle$.

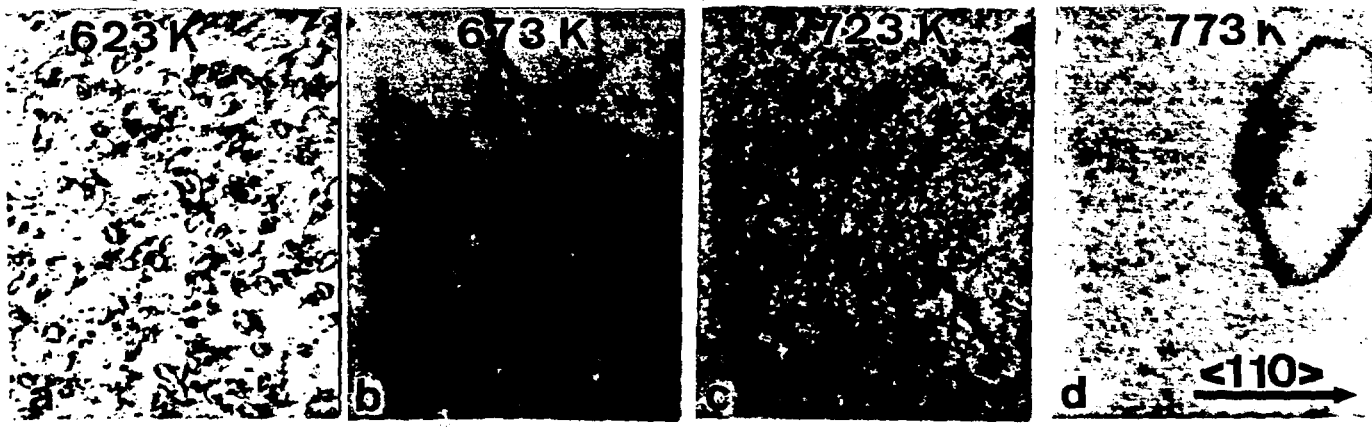

Fig. 3. Dislocation loop and network structures observed for irradiation temperatures of 623 to 773 K. $\underline{g}$ is indicated by the arrow; the length of the arrow equals 500 nm. $\underline{z} \sim \langle 111 \rangle$.

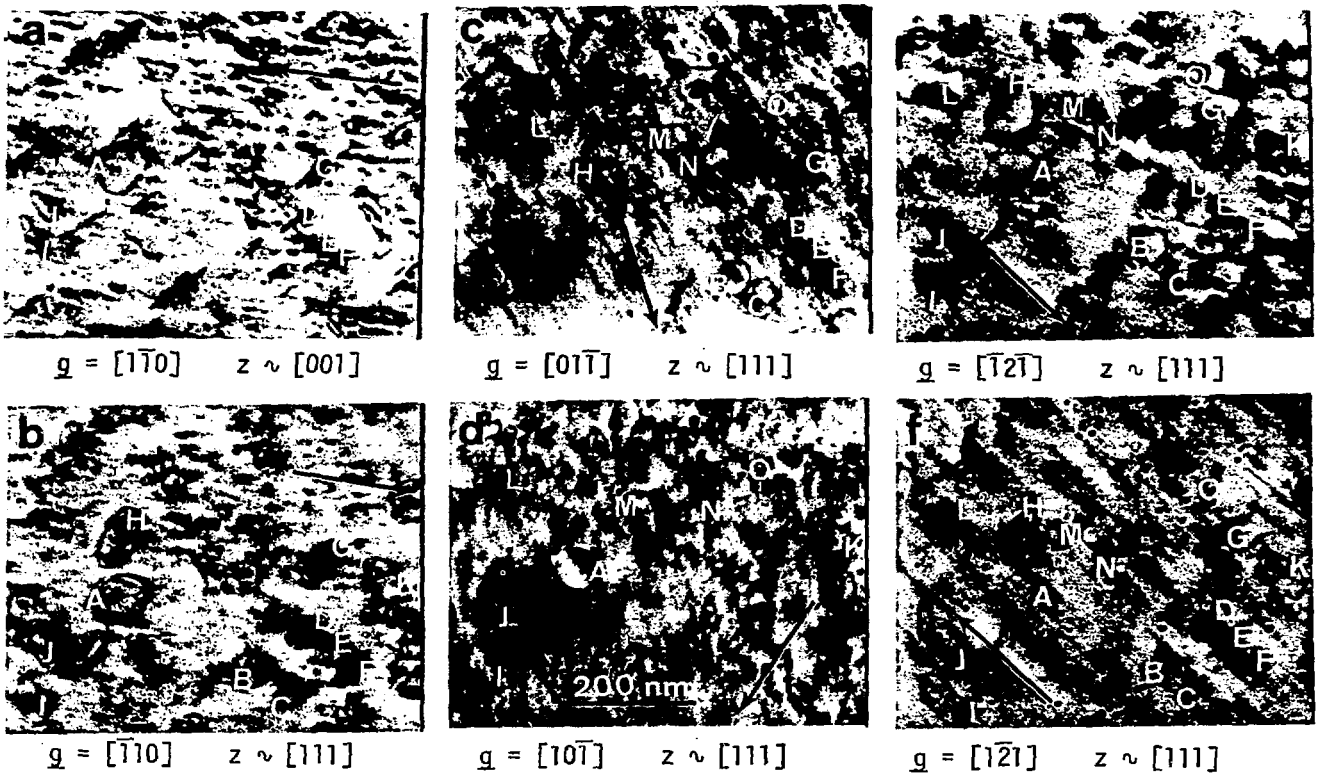

Fig. 5. Part of the analyses of the geometry and nature of the dislocation loops. T_I = 623 K. The arrows indicate g. For the loops labeled: A, b = a/2[$\bar{1}$11]; B–H, b = a[010]; I–K, b = a[100]; and L–O, b = a[001]. All are interstitial loops.

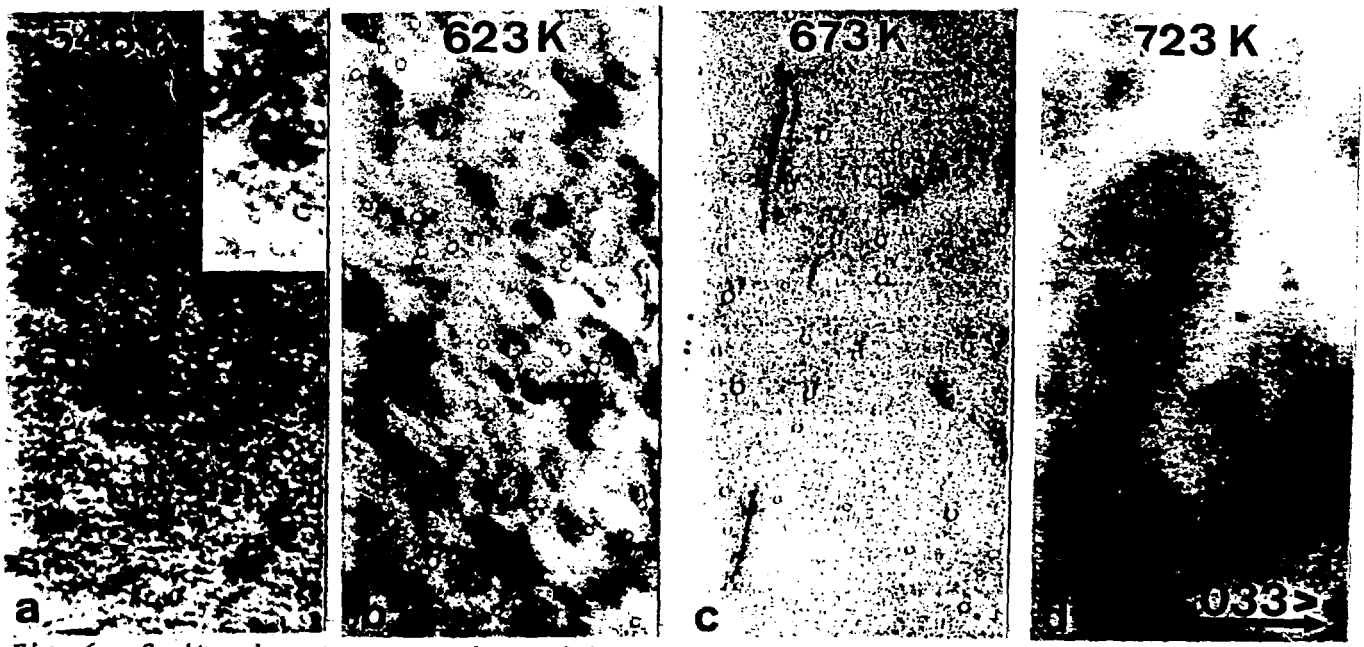

Fig. 6. Cavity microstructures observed in neutron-irradiated iron. Inset in (a) is a 2× enlargement. g is indicated by the arrow; the length of the arrow equals 200 nm. z ~ ⟨111⟩.

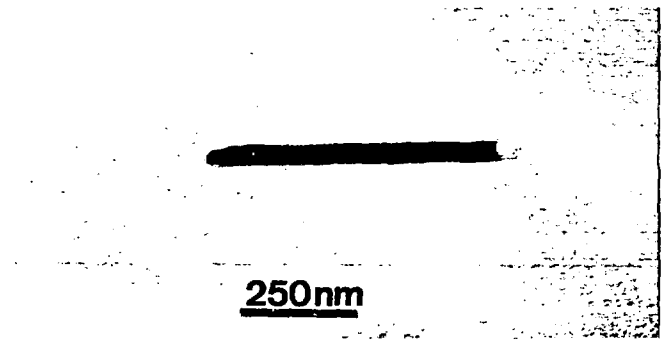

Fig. 7. Cavities observed at precipitates. T_I = 773 K.

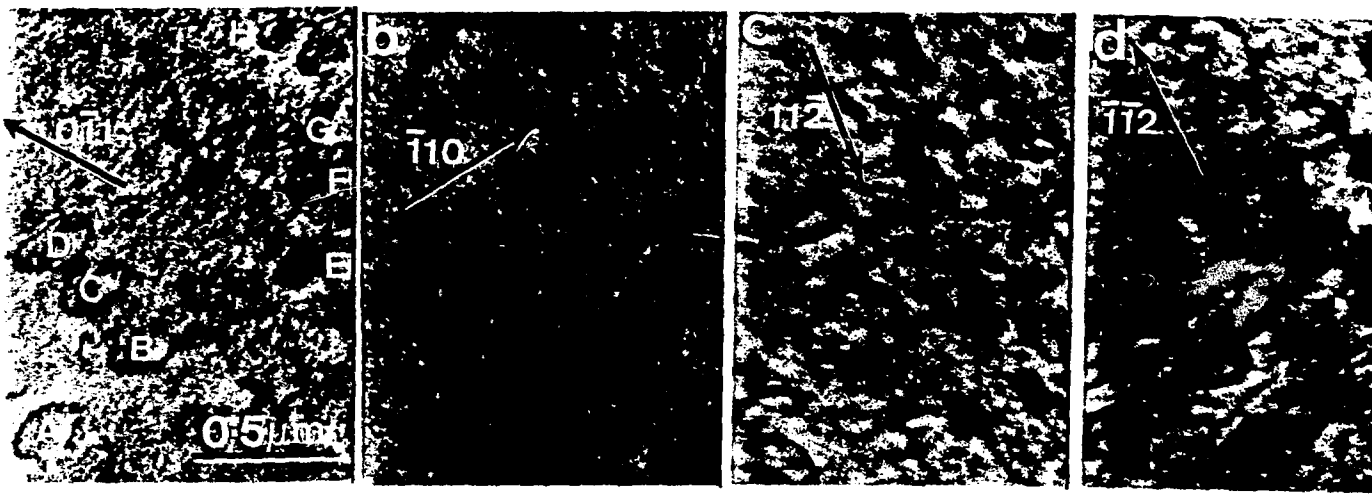

Fig. 10. Part of the analysis of the geometry and nature of dislocation loops in the halos. T_I = 723 K. Arrows indicate $\underline{g}$. For loops labeled A–H, $\underline{b}$ = a[001], interstitial loops.

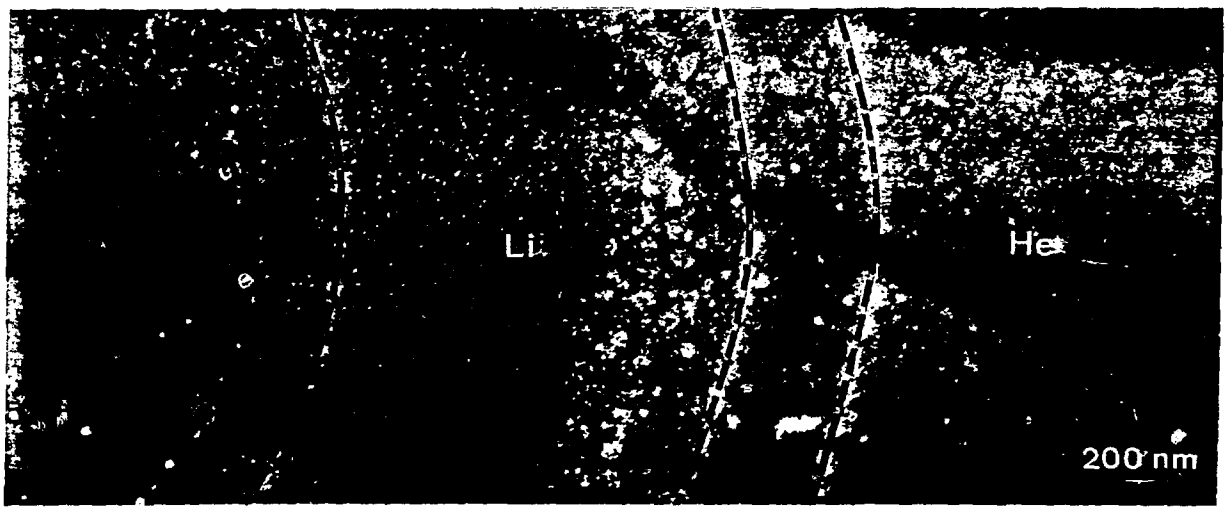

Fig. 11. Enlargement of cavity halo. The approximate extent of the helium and lithium halos are indicated by broken lines. The helium halo extends beyond the edge of the micrograph. T_I = 923 K. Etching from the electropolishing is also evident.

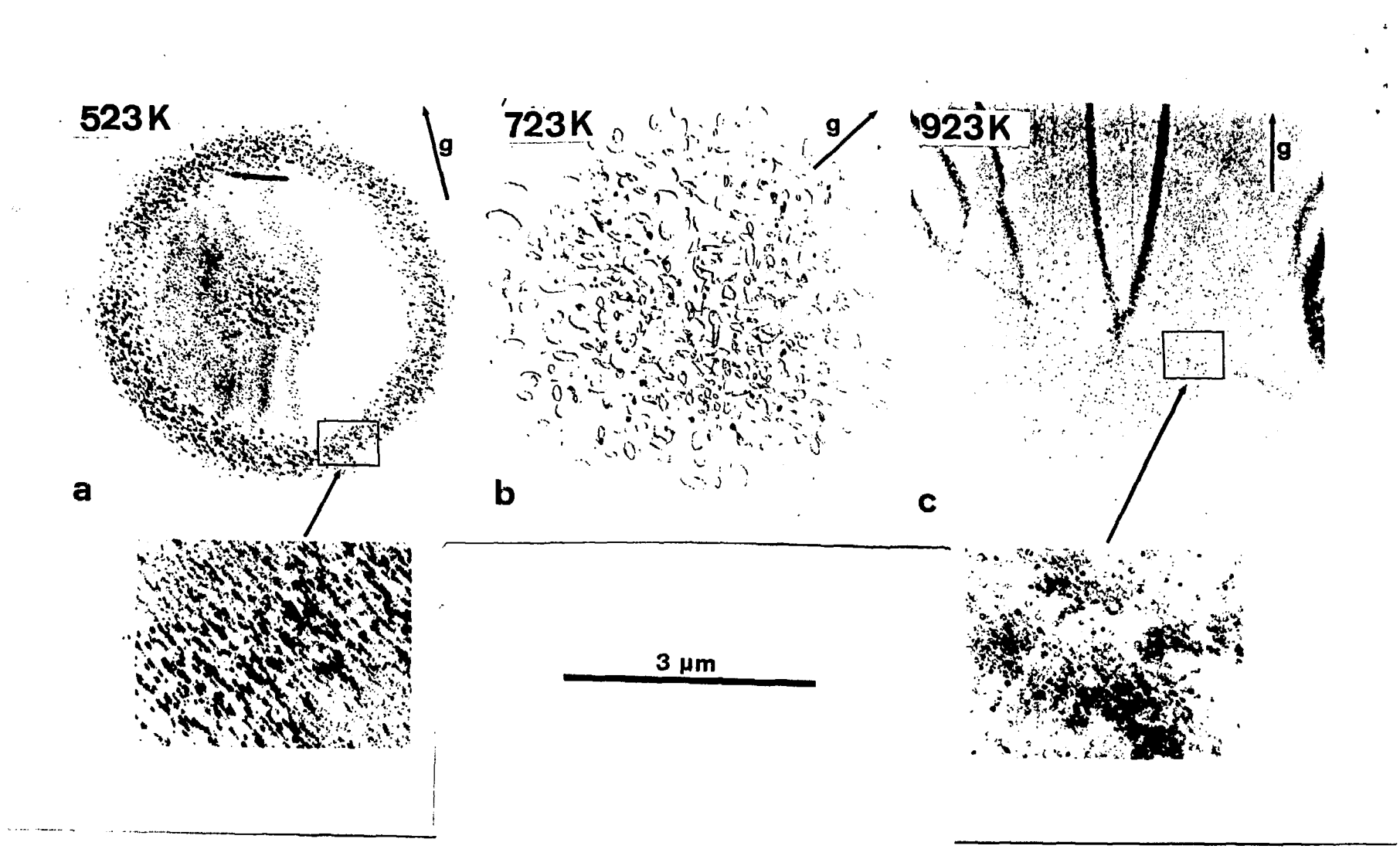

Fig. 9. Halo microstructures observed in neutron-irradiated iron. $\underline{g}$ = <110>; $\underline{z}$ ~ <111>.

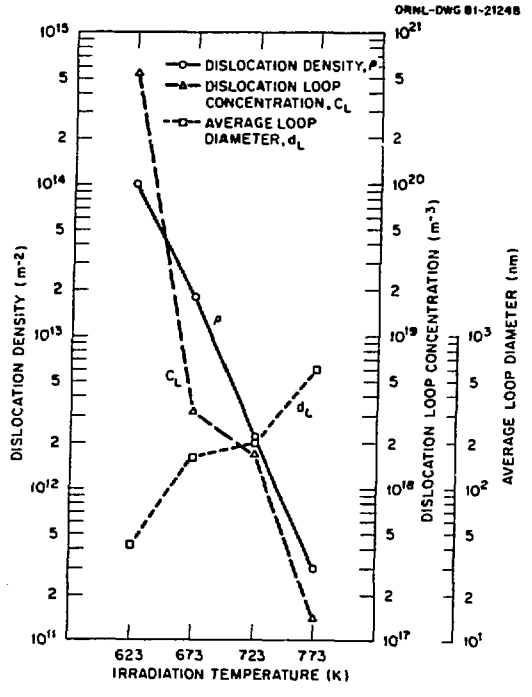

Fig. 4. Dislocation loop parameters and total dislocation density for intermediate irradiation temperatures.

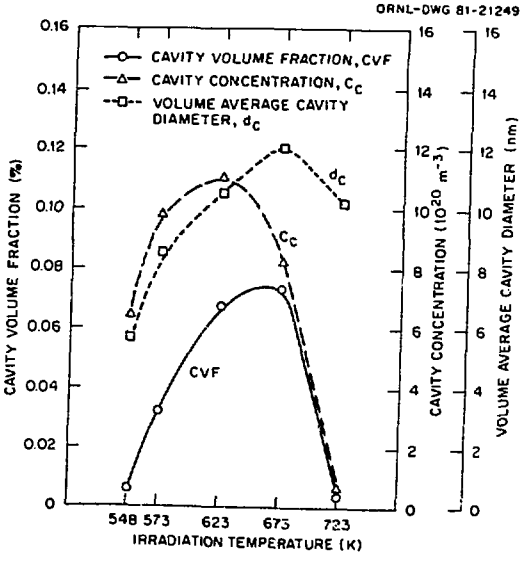

Fig. 8 Quantitative data for cavities in neutron-irradiated iron.